

This is an Open Access document downloaded from ORCA, Cardiff University's institutional repository: <https://orca.cardiff.ac.uk/id/eprint/76837/>

This is the author's version of a work that was submitted to / accepted for publication.

Citation for final published version:

Clarke, Alastair , Evans, Henry Peredur and Snidle, Raymond 2016. Understanding micropitting in gears. Proceedings of the Institution of Mechanical Engineers, Part C: Journal of Mechanical Engineering Science 10.1177/0954406215606934

Publishers page: <http://dx.doi.org/10.1177/0954406215606934>

Please note:

Changes made as a result of publishing processes such as copy-editing, formatting and page numbers may not be reflected in this version. For the definitive version of this publication, please refer to the published source. You are advised to consult the publisher's version if you wish to cite this paper.

This version is being made available in accordance with publisher policies. See <http://orca.cf.ac.uk/policies.html> for usage policies. Copyright and moral rights for publications made available in ORCA are retained by the copyright holders.



Understanding micropitting in gears

A. Clarke, H.P. Evans, R.W. Snidle

School of Engineering, Cardiff University, Cardiff, UK

Abstract

Micropitting is a serious form of erosive wear which can occur on the teeth of transmission gears. It is associated with roughness effects and surface fatigue, and has become a particular problem in the speed-increasing gearboxes of wind turbines. This paper reviews the contributions which the authors have made towards an understanding of the basic mechanism of micropitting in gears based on analysis of the contact mechanics and elastohydrodynamic lubrication (EHL) of gear tooth surfaces under realistic operating conditions. Results are presented which demonstrate the crucial influence of EHL film thickness in relation to roughness (the “lambda ratio”) on predicted contact and near-surface fatigue. The important effect of plastic deformation which takes place during the initial stage of running-in of gears has also been investigated, and it has been shown that significant residual effects occur which can contribute to the early formation of surface-initiated cracks.

Keywords: micropitting; fatigue; gears; EHL; wear.

1 Introduction

Micropitting is a type of erosive wear which appears on the working parts of gear teeth. It is generally associated with surface roughness effects in high duty hardened gears finished by grinding [1]. Damage begins in the form of small surface pits typically 10-30 μm in diameter and 5-10 μm in depth. Figure 1 shows micropitting damage on the teeth of a helical gear used in a testing programme at the Design Unit of Newcastle University. The image shows micropitting erosion occurring predominantly in the dedendum of the teeth. The term “grey staining” is widely used to describe the dull appearance of micropitting on the.

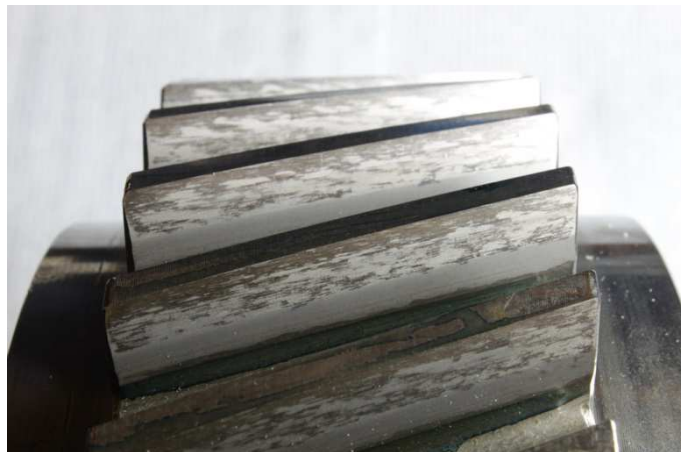


Fig. 1 Micropitting damage on the teeth of a helical test gear. (Courtesy of Design Unit, Newcastle University).

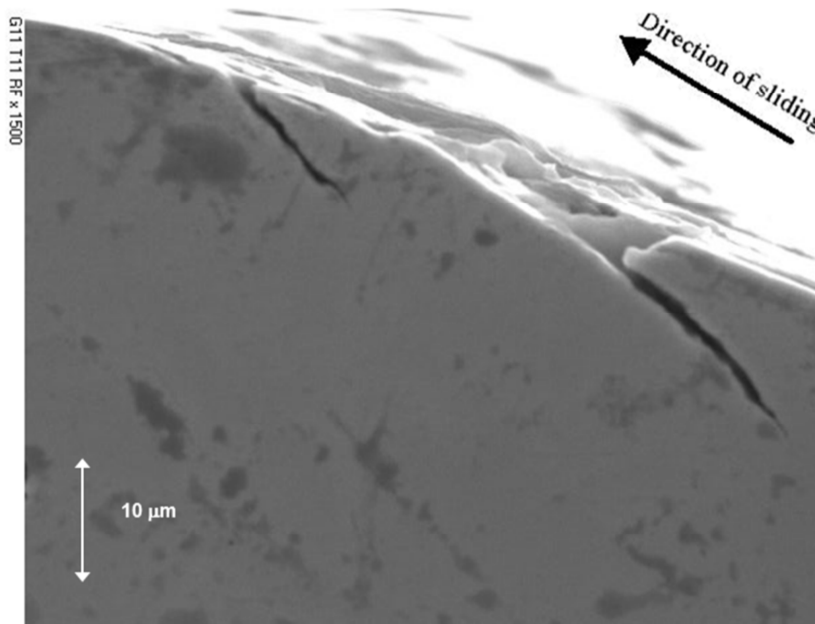


Fig. 2 Section of micropitted surface of helical gear tooth showing surface cracks and direction of sliding on the surface. (Courtesy of Design Unit, Newcastle University)

gear flank. The level of wear in this case amounts to a maximum deviation of approximately $6\ \mu\text{m}$ from the involute profile. Damage is also apparent in the addendum of the teeth but is less severe with parts of the surface remaining almost unaffected. The gear with which it meshed showed similar damage, which was again concentrated in the dedendum of the teeth. Micropitting appears to be due to surface contact fatigue and plastic deformation on the scale of roughness asperities. The initial surface distress can, in some cases, become self-arrested [2], and may even be regarded as no more than a benign kind of “running-in”. However, the shallow surface cracks may grow and lead to deeper crack-branching, which in turn can develop into larger-scale (macro) pitting. In serious cases this can cause unacceptable degradation of the gear tooth profile and even tooth breakage [3]. The initial damage occurs at the tips of surface asperities, particularly in the root (dedendum) parts of both the driver and driven gears, without necessarily causing pitting on the corresponding contacting parts of the meshing gear. The shallow cracks, as seen in the section of a micropitted gear tooth shown in Figure 2, characteristically grow in a direction which is opposite to the direction in which the sliding frictional traction acts on the affected surface, i.e. towards the pitch point on the driver tooth, and away from the pitch point on the driven tooth as illustrated schematically in Figure 3. The problem of micropitting (in both rolling element bearings and gears) has been particularly troublesome in the speed-increasing gearboxes used in wind turbines, and two international workshops [4,5] sponsored by the US National Renewable Energy Laboratory (NREL) were organised to address this specific issue, for example. The present authors contributed to the NREL workshops and have also been active participants in a British Gear Association (BGA) funded research project on “Understanding Micropitting”. This paper summarises the authors’ contribution towards finding a solution to the micropitting problem in gears based upon an improved understanding of the contact mechanics and lubrication taking place at the heavily-loaded rolling/sliding conjunction between meshing teeth.

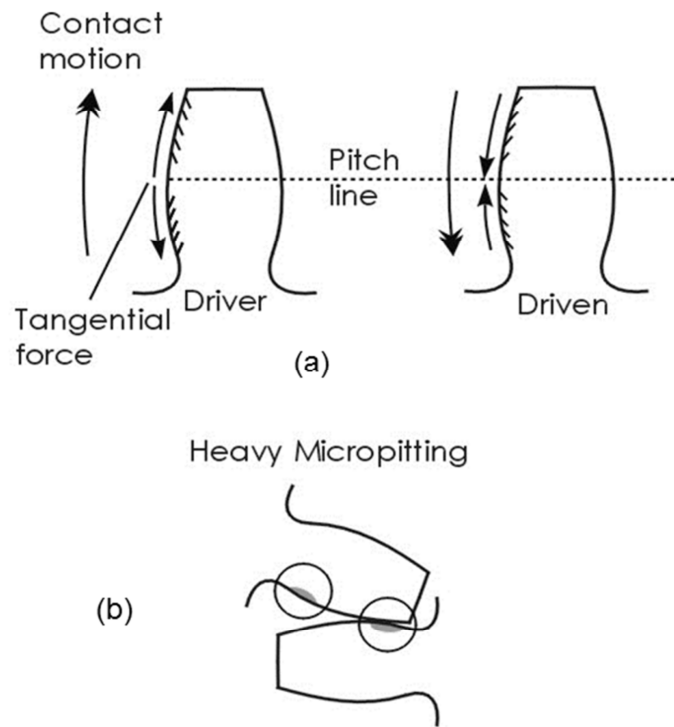


Fig. 3 Illustration of observed direction of growth of micro-cracks on gear teeth

2 Rough surface lubrication

The mechanism responsible for the effective fluid-film lubrication of heavily-loaded rolling/sliding contacts between non-conforming surfaces is elastohydrodynamic lubrication (EHL). Under ideal gear operating conditions of load, speed and temperature, and with the assumption of perfectly smooth surfaces, the classical Dowson and Higginson [6] equation predicts EHL films of the order of $1.0 \mu\text{m}$. In practice the surface roughness present on the teeth of even the best quality gears finished by grinding is typically $0.4 \mu\text{m}$ roughness average (Ra) with peak-to-valley asperity features of about $2\text{-}4 \mu\text{m}$. It is therefore inevitable that when two such tooth surfaces are in heavily-loaded rolling/sliding contact the generation of an effective EHL film will be significantly affected by roughness. Under these conditions the mechanism is referred to as micro-elastohydrodynamic lubrication (micro-EHL) in which the time-varying pressure distribution becomes sharply rippled with peak pressures at asperity/asperity encounters far in excess of the nominal peak Hertzian pressure distribution for smooth surfaces [7]. In addition the pressure ripples are narrow with a width that is commensurate with the interaction length of the asperity lands. As a result the pressure ripples cause high principal shear stress values in the material at positions proximate to the surface rather than at the depth of the nominal Hertzian pressure's peak principal shear stress. This has obvious consequences for fatigue and damage at the asperity level, which may appear as micropitting. A full physical model of micro-EHL under realistic conditions presents a serious challenge for numerical analysis, but several researchers have contributed numerical analyses of micro-EHL based upon plausible assumptions concerning elastic deformation and hydrodynamic effects. Chang and Webster [8] presented a model for line contacts (the situation occurring at the contact between cylindrical rollers or spur gears)

which included a consideration of asperity contact and took account of the transient nature of the problem due to “moving roughness”. Jiang et al. [9] and Zhao et al. [10] solved the point contact problem by dividing the overall contact area into domains of either solid contact or lubricated separation. Hu and Zhu [11] formulated a unified approach for full film, mixed lubrication, and boundary lubrication with a simplified Reynolds equation. A similar approach using a “reduced” Reynolds equation has been used by Liu et al. [12] in a mixed lubrication line contact solution for spur gears. More recently He et al. [13] have been able to solve the challenging problem of including elastic/plastic behaviour in a rough surface solver, the results of which show how the presence of plastic deformation may significantly reduce some of the pressure spikes and give a more even distribution of load support. A powerful, robust method of solving the general EHL problem which is capable of handling the most severe, thin-film/high roughness conditions was introduced by Hughes et al. [14] and Elcoate et al. [15]. The method is based on the differential deflection formulation for the elastic deformation which enables close coupling of the Reynolds and deflection equations in a rapidly-convergent solution scheme. It does not rely on a “reduced” formulation of the Reynolds equation and has the added advantage of embodying mass conservation. Holmes et al. [16] successfully modelled gear lubrication conditions in which the roughness was at least an order of magnitude greater than the minimum film thickness using this approach, and also developed the method for point contacts. [17]. The coupled solver was subsequently successfully applied to the analysis of contact conditions in helical gears used in a programme of experiments on micropitting [18].

3 Simulation of micro-EHL of gear tooth surfaces

The rough surfaces used in the results presented here were taken from profilometer traces obtained from actual test gears. The combination of rolling (entrainment velocity), relative sliding and radius of effective curvature at the contact between involute gear teeth varies continuously throughout the meshing process, and in the micro-EHL simulation it is therefore important to synchronise the opposing profiles in their correct relative positions as they roll/slide together, from start to end of the meshing cycle in order to reproduce the unique asperity/asperity interactions which take place as an asperity crosses the Hertzian contact zone. If the relative positions of the rough profiles are offset then the asperity on the fast rough surface will interact with a different set of asperities on the slow surface according to the slide/roll ratio. Considering a slide/roll ratio of 0.9, for example, shows that an offset of no more than $0.25a$ is required to ensure that 80% of the interaction length for a fast surface asperity corresponds to the actual interaction length on the smooth surface, where a is the nominal Hertzian contact semi-dimension. This alignment is achieved by measuring the profiles relative to an identifiable datum position on the tooth. It is convenient to use the tooth tip as the datum point by allowing the profilometer stylus to over-run the tooth tip during its traverse. The tooth tip then appears as a clearly, uniquely identifiable feature on the profile trace as shown at profile position 9.5 mm in Figure 4(a). When acquiring the profile the gear tooth is carefully positioned so that the independent straight-line reference of the profilometer is parallel to the tangent to the tooth at its pitch line as shown in Figure 4(b). It is then possible, using involute geometry and the basic parameters of the gears, to identify mutually contacting points on the two opposing profiles corresponding to a given state of meshing and to carry out transient elastohydrodynamic analyses incorporating the moving surface roughness of the two surfaces.

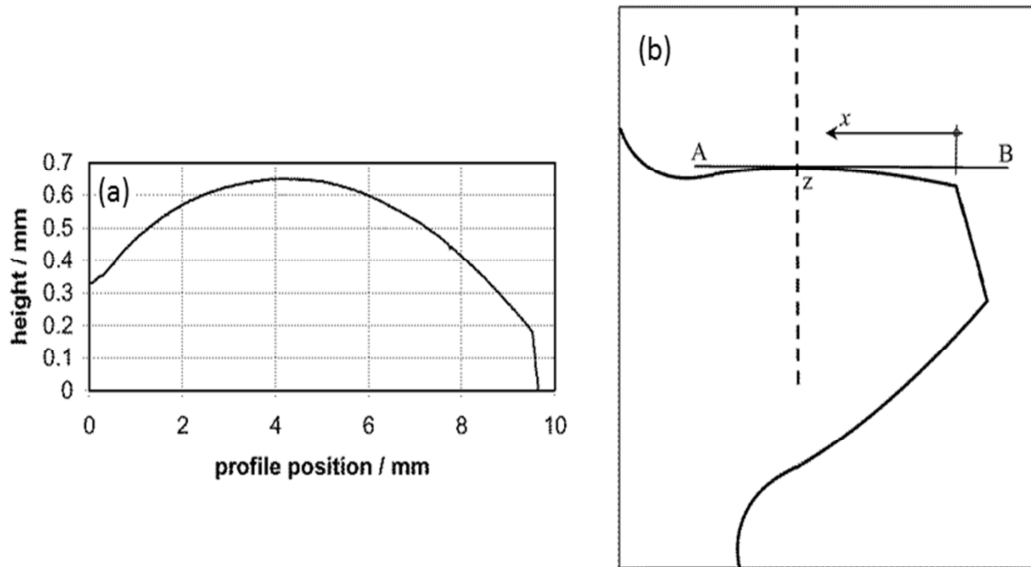


Fig. 4 (a) typical raw profilometer trace of a gear tooth showing the tooth tip location on the right (origin of the x -coordinate) (b) illustration showing the setup for measurement of the tooth profile. Here, AB is the datum line of the profilometer, which is tangential to the tooth at the working pitch point z and x is the distance along the profile measured from the tooth tip.

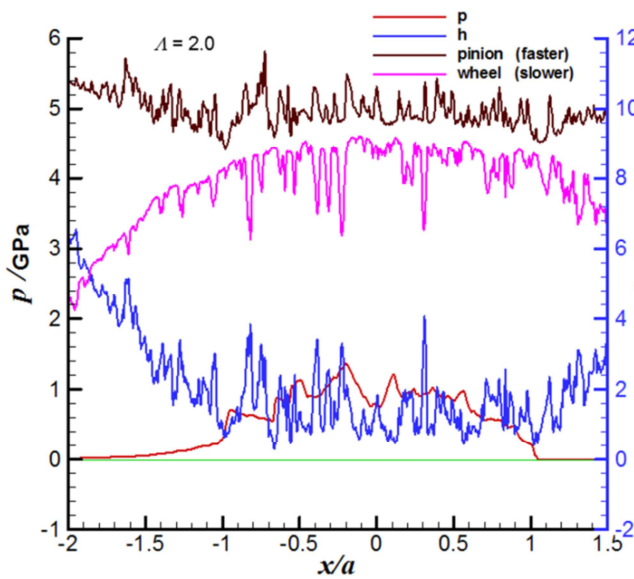


Fig 5. EHL pressure and film thickness results of simulation of micro-elastohydrodynamic lubrication of a gear tooth contact for a single timestep. Nominal Hertzian contact pressure = 1.0 GPa, $\Lambda = 2.0$.

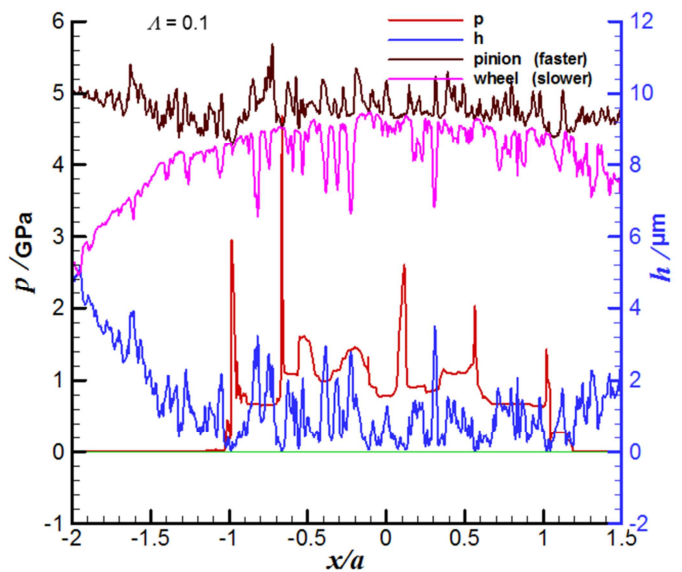


Fig 6. EHL pressure and film thickness results of simulation of micro-elastohydrodynamic lubrication of a gear tooth contact for a single timestep. Nominal Hertzian contact pressure = 1.0 GPa, $\Lambda = 0.1$.

Figures 5 and 6 show two typical results obtained from the simulation of the contact of a pair of helical gears in this way. They show results for two different values of the lambda ratio which is defined as

$$A = \frac{h_c}{\sqrt{R_{q1}^2 + R_{q2}^2}} \quad (1)$$

where h_c is the reference theoretical film thickness at the centre of the contact calculated on the assumption of smooth surfaces and R_{q1} and R_{q2} are the standard deviations of the roughness profiles of the gear teeth. A is often used as an indicator of the severity of the operating conditions, with small values of A indicating high levels of asperity interaction. The analyses illustrated in Figures 5 and 6 were carried out with the same rough surfaces but with different ambient viscosity values, so as to produce results for different A values for the same kinematic conditions. The figures illustrate the same timestep in each analysis and show the pressure, p , and film thickness, h , together with the individual rough surfaces above, which are offset by about 9 μm for clarity. The operating conditions in Figure 5 correspond to a calculated A value of 2.0 and it can be seen that the rough surfaces are effectively separated by a coherent lubricant film. The corresponding maximum Hertzian pressure, for smooth surfaces, in this case is 1.0 GPa, but pressure ripples of almost twice this value are present even under these relatively favourable conditions. A far more severe condition is illustrated in Figure 6 for the same rough surfaces. In this case the A value is reduced to give a predicted value of 0.1 by operating at a lower entraining speed. The rough surfaces are now seen to be in much closer interaction, and intermittent “dry” contact is predicted at the worst locations of asperity/asperity interactions. The effect on the pressure profile is dramatic, with predicted localised pressure spikes of over three times the corresponding maximum Hertzian value occurring at positions of aggressive asperity interactions. It becomes clear from these simulations that when operating under thin film conditions the possibility of damage due to both contact/adhesion and severe high pressure loading is greatly increased.

4 Experiments on mixed lubrication

The occurrence of mixed lubrication under gear operating conditions has been investigated experimentally using an electrical contact resistance technique. One of the first users of this method was Crook [19] who made contact measurements in a disc machine. It was found that contact events diminished rapidly during running-in. In a widely cited article Furey [20] described the transient nature of electrical contact in a ball-on-cylinder experiment and introduced the concept of the time-averaged value of contact resistance as an indication of the percentage time for which metallic contact occurred. Talian et al [21] carried out similar experiments using a four-ball rig and developed two representative parameters: the average no-contact time fraction, and the average number of contacts per unit time. Further enhancements to the technique were reported by Leather [22] who developed statistical techniques to deal with simultaneous contacts, and Palacios [23] who was interested in the effect of running-in on electrical contact. Guangteng et al [24] made measurements of both film thickness (using optical interferometry) and electrical contact resistance over a range of operating conditions which showed that the electrical contact resistance fluctuated rapidly with distinct intermediate levels of resistance between high levels associated with full film EHL and low values corresponding with asperity contact. Lugt et al [25] carried out disc machine tests in an investigation of running-in of bearing rollers. They found that the contact voltage was directly proportional to the level of separation. They also noted that the contact voltage gradually increased with running time, which was taken to be indicative of surface improvement by the running-in process. Lord and Larsson [26] carried out electrical contact resistance tests in which a smooth steel ball was loaded against a rougher steel disc. They introduced the concept of the “lift-off” test which shows the way in which the percentage contact time falls rapidly with increasing speed following a period of running-in, thus

demonstrating the transition from mixed to full film lubrication. With the exception of some of the earlier work on contact resistance most workers have used the mean contact resistance to indicate the state of the film. In our own work we have concentrated attention on the transient behaviour of contact voltage between discs in a two disc rig under heavily loaded conditions typical of gear tooth contacts. A photograph of the main parts of the rig is shown in Figure 7. The “slow” disc shown in this figure is electrically insulated from the rest of the rig by means of a PEEK bush in its drive coupling and hybrid ceramic/steel ball bearings in the pivot of the swinging yoke. Insulation is also provided in the coupling to the slow disc slip ring and the loading push rod which is visible on the right of the figure. The discs are crowned and finished by axial grinding with a roughness average (Ra) of approximately $0.4\ \mu\text{m}$ to simulate gear tooth finish in terms of both roughness and its lay relative to the direction of rolling/sliding. The discs were manufactured from alloy steel to Rolls-Royce specification RR6010, gas-carburised and hardened. Tests were also carried out using superfinished discs with an Ra of less than $0.1\ \mu\text{m}$. The discs were lubricated with a naval gear oil meeting specification OEP-80 with a nominal viscosity of 68 cSt at $40\ ^\circ\text{C}$ which contained a proprietary extreme pressure additive. A voltage of 43 mV was applied between the discs using a potential divider network. Electrical connections to the two discs were made via silver-graphite slip-rings. A high speed data acquisition system operating at a speed of 1.25 MHz was used to capture the rapidly varying voltage measured across the disc contact. The discs were gear-connected to give a realistic slide/roll ratio of 0.25, and a high-resolution shaft-encoder was fixed to the faster disc. In this way it was possible to acquire the contact voltage over a complete rotation of the disc with repeated rotations triggered at the same angular position. The slide/roll ratio was achieved with a gear ratio of 7:9 so that the same points on the two discs came into repeated contact every nine rotations of the fast shaft (other slide/roll ratios ranging from zero to 1.0 obtained by changing the gears on the two shafts). It was then possible to assess the repeatability of the voltage signal and thereby monitor detailed changes occurring as a result of running.

Figure 8 shows three contact voltage traces, representing 90 degrees of rotation of the fast disc, taken nine rotations apart. In this test the surfaces were superfinished and the operating conditions were typical of a heavily loaded gear tooth contact running at a moderately low speed (maximum Hertzian contact pressure 1.4 GPa; entrainment velocity 1.42 m/s; oil feed temperature $50\ ^\circ\text{C}$). The voltage is seen to oscillate rapidly between the upper and lower limits corresponding to full film and metallic contact, respectively. The repeatability of the traces indicates that the voltage response is due to identifiable regions of asperity/asperity encounters, and that for the majority of the time a full film is present over the whole of the nominal elliptical contact area which is, at the operating load, about $2.5\ \text{mm}^2$. In the three

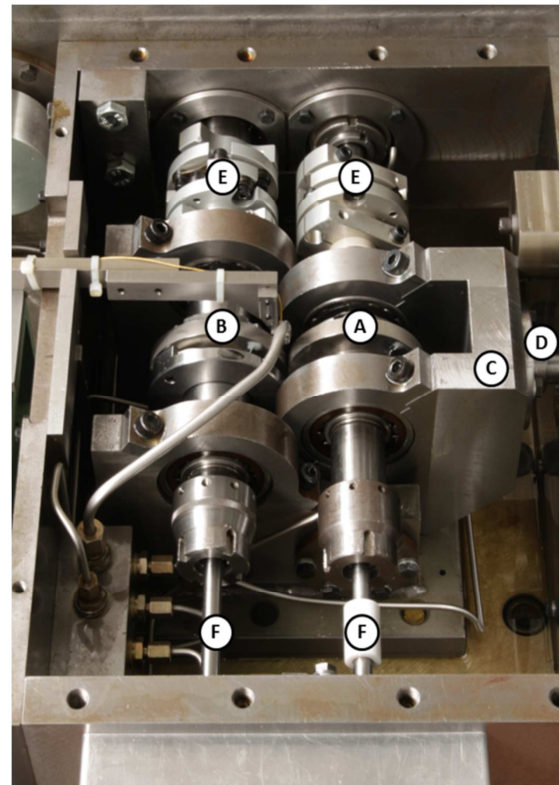


Fig 7. Photograph of test head of disc rig. A slow disc; B fast disc; C swinging yoke; D loading push rod; E torsionally-rigid couplings; F slip ring connections to embedded thermocouples and electrical contacts.

traces shown the mean contact voltage was calculated to be 20 mV, 18 mV and 17 mV, respectively. Repeated voltage traces taken at the same position of the fast disc at every 10th contact, so that the counterface roughness is different at each pass, show significantly less correlation. Experiments with rougher surfaces showed a far greater degree of contact, and it was only at higher speeds that full film conditions were indicated. Experiments were carried out at a range of loads (1.0 GPa to 1.4 GPa) and entraining velocities (0.71 m/s to 7.1 m/s) in which both mean contact voltage and friction coefficient were measured. The collected results are summarised in Figure 9 as a function of the calculated λ ratio. The data plotted in Figure 9 were generated using two axially-ground discs with stable Ra values of 0.35 μm and 0.32 μm following running-in at steadily more aggressive conditions (reaching the highest load and lowest speed used in this work) such that the surfaces were stable under all conditions encountered in the test programme. The discs were run until steady-state temperatures were achieved at a range of speeds and loads, at a slide/roll ratio of 0.25, giving the range of λ ratios shown in the figure. The λ ratio is often cited as an indicator of the effectiveness of EHL in preventing wear and damage in lubricated contacts. In carefully controlled laboratory experiments in which film thickness was measured using the optical interferometry method it was concluded that full-film EHL (as predicted on the assumption of smooth surfaces) is only achieved when λ has a value of 2 or greater [27]. In the case of the elliptical contact used in our experiments the reference theoretical film thickness used in the

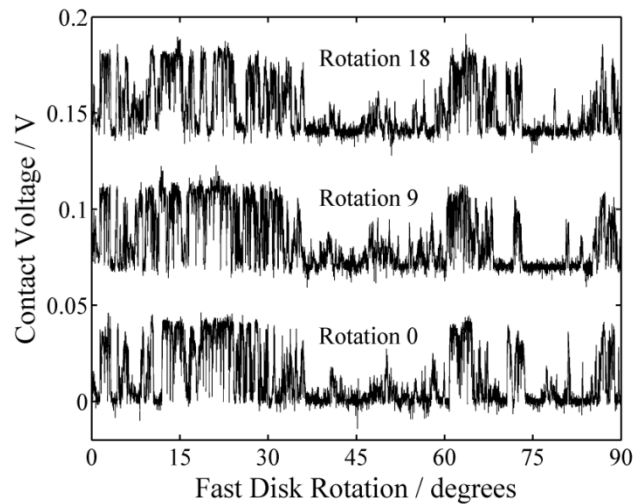


Fig. 8 Variation of contact voltage during a repeated 90° rotation of the fast disc. The figure shows three traces taken at rotation 0, rotation 9, and rotation 18 of the disc. The second and third traces are offset by 0.07 volts and 0.14 volts, respectively, for clarity. Both discs were superfinished. Maximum contact pressure = 1.4 GPa; speed of fast disc = 200 rev/min.

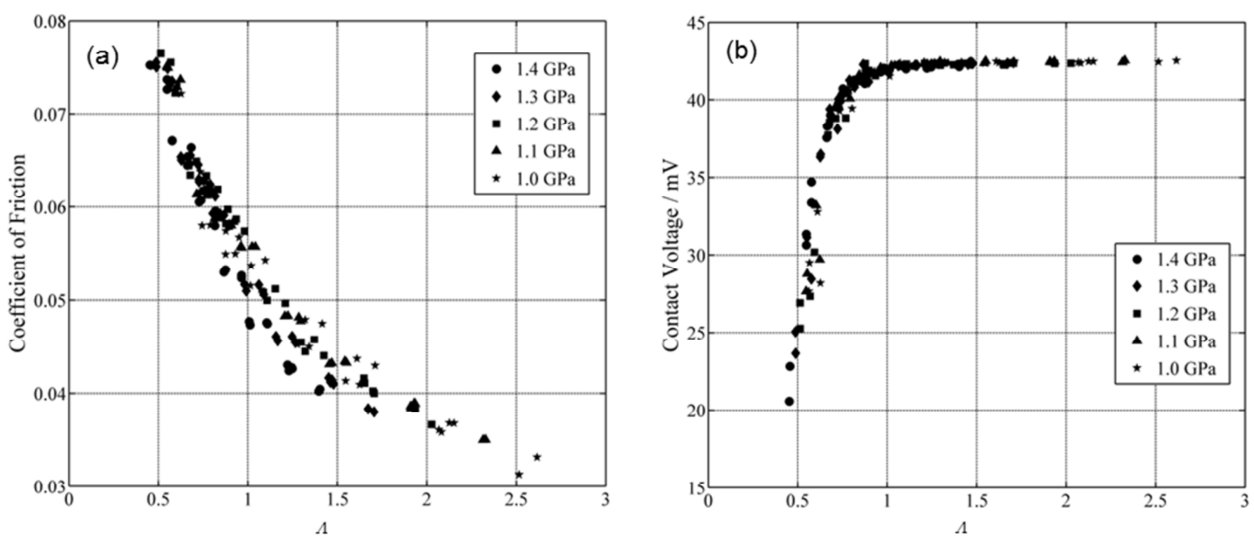


Fig. 9 Measured values of friction coefficient versus λ ratio for a range of loads and speeds at a slide/roll ratio of 0.25.

above formula was obtained from the empirical formula of Chittenden, et al. [28]. In Figure 9 it can be seen that the approach to full film behaviour is indicated only when λ reaches about 1.5. The coefficient of friction shown in Figure 9 (a) follows a steady decline with increasing speed (and λ) demonstrating the transition from mixed lubrication to conditions approaching full EHL. Figure 9 (b) shows that mean contact voltages only approach 43 mV for $\lambda > 1.5$, indicating that at lower values of λ there are increasing levels of direct metallic asperity interaction taking place. These experimental results strongly support the view based on the optical EHL experiments conducted independently by others that the λ ratio provides a good guide to the effectiveness of the EHL film; further theoretical evidence of the value of this ratio as a predictor of near-surface fatigue damage will be presented in the following sections of the paper.

5 Modelling of fatigue in lubricated, rough surface contacts

Detailed results from the transient micro-EHL solutions can be used to predict conventional high-cycle fatigue damage in the vulnerable thin surface layer. At each timestep in the solution process stored values of pressure, film thickness and surface traction are used to calculate the instantaneous distribution of subsurface elastic stress and strain components from the following convolution integrals.

$$\begin{aligned}\tau_{xz} &= -\frac{2z^2}{\pi} \int_{p>0} \frac{p(s)(x-s)ds}{((x-s)^2 + z^2)^2} - \frac{2z}{\pi} \int_{\tau>0} \frac{\tau(s)(x-s)^2 ds}{((x-s)^2 + z^2)^2} \\ \sigma_z &= -\frac{2z^3}{\pi} \int_{p>0} \frac{p(s)ds}{((x-s)^2 + z^2)^2} - \frac{2z^2}{\pi} \int_{\tau>0} \frac{\tau(s)(x-s)ds}{((x-s)^2 + z^2)^2} \\ \sigma_x &= -\frac{2z}{\pi} \int_{p>0} \frac{p(s)(x-s)^2 ds}{((x-s)^2 + z^2)^2} - \frac{2}{\pi} \int_{\tau>0} \frac{\tau(s)(x-s)^3 ds}{((x-s)^2 + z^2)^2}\end{aligned}\quad (2)$$

The stress history at each point in a representative block of material is broken into a series of loading cycles and a corresponding degree of damage calculated for each cycle. The rainflow counting method [29] gives the effective load cycles and the corresponding stress levels for each cycle. Different models are available for calculating the damage sustained at each loading cycle, but they have been found to differ little in their predictions [30]. The method currently adopted in our work is that proposed by Fatemi and Socie [31] and is expressed by equation (3) which gives the number of loading cycles to failure N_f for the effective loading cycle.

$$\gamma_a \left(1 + K \frac{\sigma_{n,max}}{\sigma'_{max}}\right) = \frac{\tau'_f}{G} (2N_f)^b + \gamma'_f (2N_f)^c \quad (3)$$

In the above γ_a is the shear strain amplitude on the material plane under consideration for the effective loading cycle, and $\sigma_{n,max}$ the maximum tensile stress normal to the plane during the effective loading cycle. The material constants in the equation can be chosen corresponding to different steels, and in our work we have taken values corresponding to SAE4340 as given by Zahavi and Torbilo [32], for example. The damage sustained in one effective load cycle is N_f^{-1} and the total damage, D , is the sum of the damage for each effective load cycle. Further details of the model are given in [31, 33]. The value of D resulting from one gear meshing cycle is obtained for each point in the material considered. Fatigue failure is assumed to occur when D reaches a value of unity, so that at any point in the material, the reciprocal of D is the number of gear meshing cycles associated with fatigue at that point.

The situation in which a full EHL film can be generated is unlikely to occur in practical gears unless they operate at high speed or have very finely-finished surfaces. It is therefore of interest to examine the effect of the Λ ratio on predicted near-surface fatigue with the aim of advancing a tentative lower limit of the Λ ratio for the avoidance of micropitting. The predicted effect of the Λ ratio on near-surface fatigue can be examined by carrying out the above fatigue simulations by varying the lubricant viscosity (other conditions remaining the same) corresponding to a range of conditions varying from “full film” to severe thin-film operation typical of heavily loaded gears at a high temperature. Damage maps corresponding to Λ values of 2.0 and 0.1 are shown in Figure 10 (b) and 10 (c), and the corresponding profile of the surface is shown in Figure 10(a). These results correspond to a short, shallow section of the surface of a pinion tooth. The colour code varies from blue ($D < 10^{-10}$ the darkest colour) to red ($D > 10^{-6}$) which is also relatively dark, and the figure is therefore best viewed in colour. The volume shown is of depth $0.2a$ and length $2a$, where a is the semi-dimension of the corresponding Hertzian line contact. This is the region of the tooth profile sub-surface material that experiences aggressive stress cycling due to the mixed lubrication effects. There is another, deeper, zone ($0.7a$) where high level stress cycling due to the average Hertzian pressure occurs, but that is not associated with micropitting. It is potentially less vulnerable to surface weaknesses, the possible development of internally pressurised cracks, and the effects of asperity plastic deformation and the associated residual stress fields. At the $\Lambda = 2$ condition the highest damage value in the figure is $D = 10^{-6}$ very near the surface at $x/a = 0.015$. At the lower Λ value there are two much larger high damage areas where $D > 10^{-6}$ centred at $x/a = 0.015$ and at $x/a = 0.12$, and new $D = 10^{-6}$ hotspots very close the surface at $x/a = -0.45, 0.40, 0.49$ and 0.80 . All of these locations of high damage can be seen to align with the prominent surface asperities. The zones of high damage are slightly offset from the corresponding asperities in some cases which is a consequence of local hydrodynamic action in which the peak hydrodynamic pressure tends to occur at the exit of micro-EHL contacts.

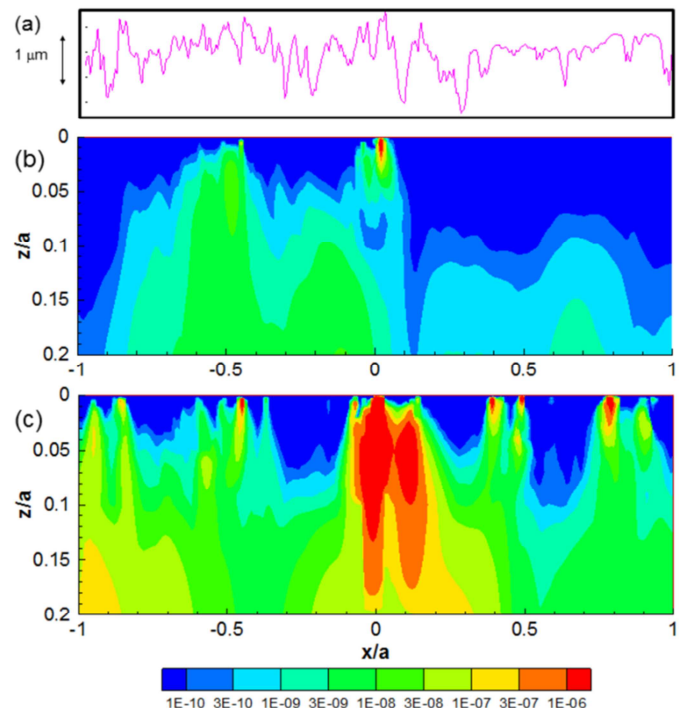


Fig. 10 Roughness profile (a) and predicted fatigue damage based on micro-elastohydrodynamic lubrication simulations of the contact of gear tooth profiles, (b) $\Lambda = 2.0$; (c) $\Lambda = 0.1$.

6 Plastic deformation and running-in

When newly manufactured gears are put to work the surfaces of the teeth undergo a process of “running-in” during which their surface profiles are noticeably modified. The highest peaks are reduced in both amplitude and tip curvature, and as a result the surfaces are able to bear the load with lower extreme pressures. It appears that the improvement in the surface can occur very rapidly. For example, in earlier tests using circumferentially-finished discs in scuffing experiments [34] it was found that varying the length of time for which the discs were run-in at each load stage (ranging from 0.5 min to 10 min) had no significant effect on the subsequent scuffing behaviour. In more recent work using axially ground discs in which re located profiles from the same parts of the discs were carefully monitored over a period of time it was found that running-in occurred in, literally, a few rotations of the discs, and that subsequent running over a far longer period, produced no further noticeable change in the surface [35]. A series of relocated profiles taken from the surface of an axially-finished disc at different stages of running at the same load is shown in Figure 11. Load was applied to the test discs for 27 seconds after which the discs were cleaned and surface profiles taken in-situ at the same circumferential positions. The profiles taken at the end of each of these 27 s load stages were relocated to align the deep valley features and compared. Figure 11 shows a detailed comparison of three such traces for a 0.15 mm length of the roughness profile. The most significant plastic deformation of the aggressive asperities can be seen when comparing the original, as manufactured, surface with that taken after the first load stage. Differences between the surface geometries following the first stage of running and the third stage are seen to be negligible, and are of the order of the measurement accuracy of the in-situ surface profilometry technique used.

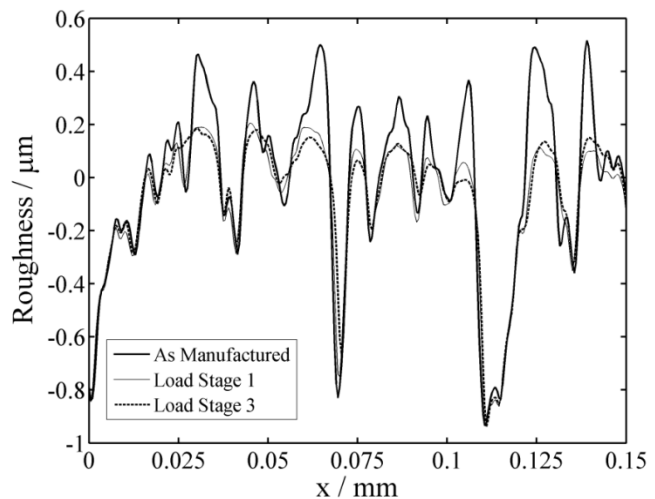


Fig 11 A series of re-located profiles taken from the fast disc showing the effect of running time on the development of surface deformation. Maximum Hertzian contact pressure = 1.7 GPa; fast shaft speed = 1500 rev/min; slide/roll ratio = 0.5; each load stage is 27 seconds in duration.

These findings strongly suggest that the changes in surface topography which occur during initial running-in are due to virtually instantaneous plastic deformation of the most prominent asperities. (Further running-in due to changes in operating loads and temperatures can also occur.) This idea of rapid asperity shape change is further supported by the results of elastic, dry contact simulations which show that when newly-manufactured ground surfaces are brought together at typical operating loads of the order of 1.0 GPa nominal Hertzian maximum pressure, the maximum local pressures at asperity contacts (based on the elastic assumption) far exceed the hardness of the steel involved. Significant plastic deformation at the asperity level would therefore seem to be inevitable when newly-manufactured gear tooth surfaces are put to work. Reduction in the height of prominent surface asperities *per se* is clearly beneficial in terms of hydrodynamic lubrication, but when this is due to significant plastic straining it may be associated with damage in the form of micro-cracks. Oila et al [36] carried out detailed metallurgical examination of a number of micropitted gears and identified what the authors called “plastic deformation regions” (PDRs) which developed beneath

asperities, and it was concluded that the intersection of the metallurgically weak boundary of the PDRs with the surface represents a critical zone from which microcracks initiate. It was suggested that these cracks then propagate preferentially along the boundary of the PDR until they reach the surface again, whereupon a micropit is created. The test gears used here and in other gear experiments reported in the paper were manufactured from 16MnCr5 steel, gas case carburised and hardened to a surface hardness of 650-750 HV before being finish ground.

Even if plastic deformation at the asperity level does not cause immediate cracking the possible creation of a tensile residual stress field in the near-surface of the asperity as a result of plastic straining may also have a significant influence on subsequent high cycle fatigue behaviour. The inclusion of elastic/plastic deformation in a full micro-EHL simulation presents significant numerical difficulties. At the current stage it has therefore been assumed that under heavily loaded conditions the elastic/plastic contact behaviour under lubricated conditions can be modelled as that between surfaces in dry contact. Considerable progress has been made in the elastic/plastic modelling of single asperities using commercial FE packages. Mulvihill et al [37] have produced an impressive FE model of the sliding frictional contact of a single pair of asperities, both spherical and cylindrical. In our own work we have investigated residual effects in the contact of both regular wavy surfaces and real surfaces [38, 39] by simulating the contact of representative lengths of profiles taken from freshly ground gear tooth surfaces. The advantage of simulating the contact of surfaces having multiple protuberances, rather than that of single isolated features, is that the possibly important effects of interaction of the stress fields of closely adjacent asperities can be revealed.

Figure 12 shows a typical result obtained from the elastic/plastic contact simulation of the test disc used for Figure 11. (The deep valley feature shown at $x = 0.063$ mm in Figure 11 appears at $x = 1.033$ mm in Figure 12). The surface profile is superimposed on a 38 mm radius circle to form a 2D deformable part. It is loaded in plane strain against a rigid plane that is

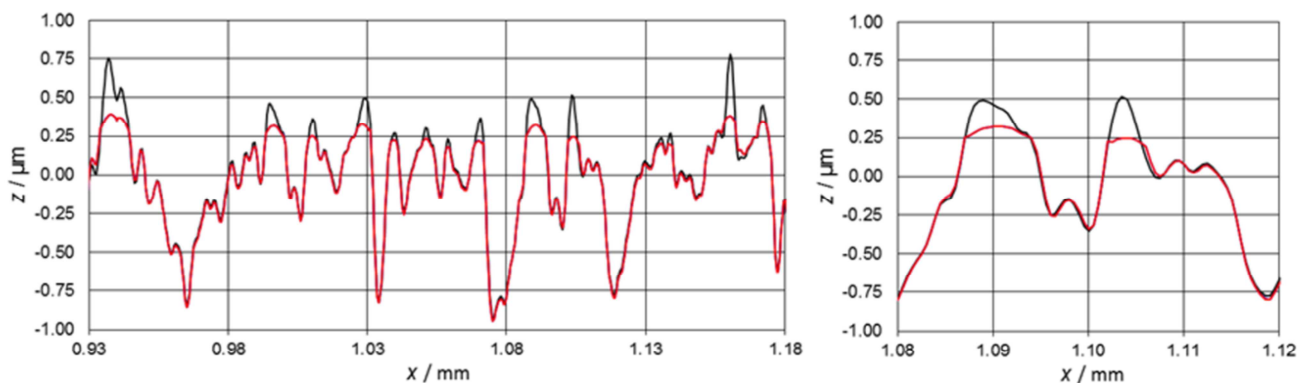


Fig 12 As manufactured roughness profile (black) with residual roughness profiles after first load application (blue) and second load application (red). The residual profiles are essentially coincident at the scale of the figures. Right hand figure shows two asperities in greater detail..

tangential to the disc at its crown. This is equivalent to loading the disc against a mirror image of itself. An elastic/plastic model is used for the material and the load applied is such that the resulting plastic deformation at the asperities is of the same order as that observed from comparison of the measured disc centreline roughness profiles. Figure 12(a) shows a 250 μm length of the profile and Figure 12(b) shows a shorter (40 μm) length of the same profile in more detail. The figures show the as-manufactured profile and the residual shape of

the roughness profile after the load is applied, and also after a second application of the same load. The two residual profiles are almost identical (less than 4 nm difference in the curves shown) which shows that there is an insignificant amount of further plastic deformation of the asperities due to the second application of the load. Simulation of further loading/unloading/loading cycles at the same load shows that the residual plastic deformation at the asperities occurs almost entirely in the first loading event. It was also found that when a higher load was subsequently applied the residual deformation was almost exactly the same as when only the higher load was applied. This theoretically predicted behaviour is confirmed by the monitored running-in experiments described above.

The stresses arising from elastic/plastic contact during loading and following removal of the load are illustrated in Figures 13 and 14. The von-Mises equivalent stress distribution in a short length of rough surface whilst under load is shown in Figure 13. In this figure the assumed yield stress was 1.6 GPa and the red area shows where plastic yield is present. These positions can be seen to correspond to the parts of the corresponding profile shown in the upper part of the figure where significant residual deformation of asperity features has occurred. The effect of plastic deformation on residual stress is illustrated in Figure 14(a) which shows the maximum positive residual principal stress vectors. It seems possible that the predicted occurrences of high residual tensile stresses at the surface can cause the initiation of shallow cracking consistent with the observed appearance of micropitting. Figure 14(b) shows contours of the maximum principal residual stress. The dashed, enclosed curve in Figure 14 is the (approximate) boundary of the zone where the maximum principal stress is positive, so that the material inside the curve has a residual stress that is compressive in all directions. The dashed curve has also been added to Figure 13 for comparison. The FE model presented here considers only normal, frictionless contact. A more sophisticated model of a tangential encounter between a single pair of “asperities” has been presented by Mulvihill et al [37] as mentioned earlier.

7 Discussion and conclusion

Detailed numerical modelling of the elastohydrodynamic lubrication of rough surfaces under gear tooth contact conditions shows that the local pressures experienced at the encounters between run-in surface asperities are far higher (often by a factor of three or more) than expected on the basis of the assumption of smooth surfaces. Hence although the presence of a thin micro-EHL film may be sufficient to prevent actual metal-to-metal contact between asperities it does not significantly “cushion” the effect of roughness on the pressure profile. Even under the most favourable conditions in which the nominal film might be twice the combined roughness ($\lambda = 2$) the effect of roughness is still clearly evident in the resulting pressure profile (see Figure 5). In the operating environment more typical of most types of present-day gears (including wind turbine gears), in which the λ ratio may have a value significantly less than unity, the pressure profile becomes very sharply rippled, and is completely unrecognisable as Hertzian under severe thin-film conditions (see Figure 6). The effect on near-subsurface time-varying stresses and predicted fatigue is dramatically increased under these conditions. Furthermore, the frequency of the short-lived transient occurrences of loss of the micro-EHL effect during the more aggressive asperity collisions increases, which adds the risk of possible local adhesion and micro welding/tearing (micro-scuffing). The presentation of predicted sub-surface fatigue damage as shown in Figure 10, for example, indicates the striking quantitative effect of reduced film-forming on predicted fatigue. Peak damage values in the near-surface layer in the case considered are typically predicted to increase by about three orders of magnitude when the λ ratio is reduced from 2 to 0.1.

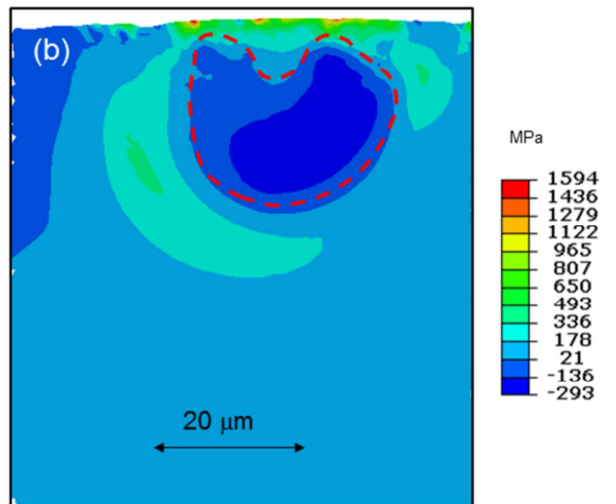
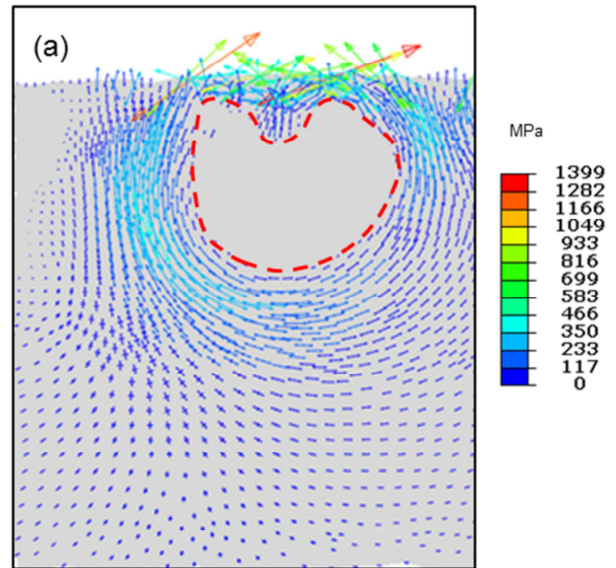
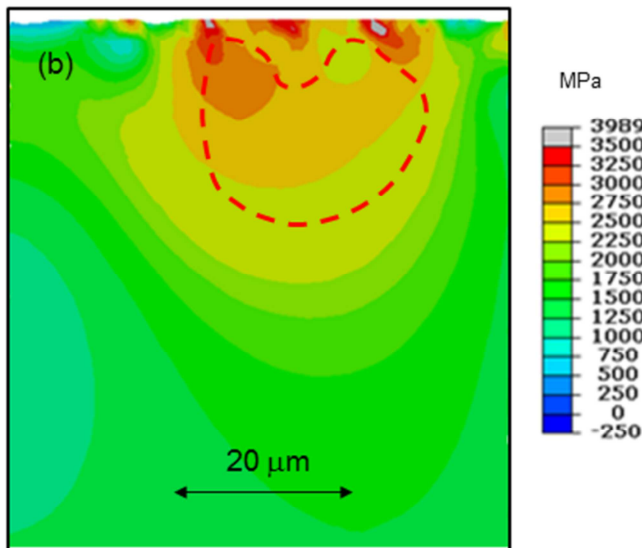
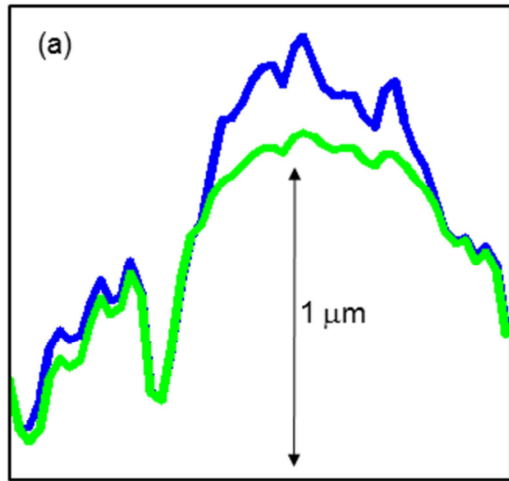


Fig 13 (a) Asperity shape before (blue) and after elastic plastic loading (green) with (b) von Mises stress under load. Dashed curve superposed from Fig 14.

Fig 14 (a) Maximum positive residual principal stress vectors with (b) contours of maximum principal stress. Dashed curve indicates boundary of zone where maximum principal stress is negative.

The results of the electrical contact resistance experiments carried out under gear operating conditions over a wide range of λ ratio in a disc machine lend support to the earlier results of direct measurements of film thickness obtained using optical measurements, and are also consistent with the predictions of fatigue damage outlined above. Repeatability of contact voltage traces when the test discs are in the same relative position clearly demonstrates the interaction of potentially identifiable asperities or groups of asperities on the two surfaces as they re-encounter one another. Although considerable interaction apparently takes place under the most severe thin-film conditions it is perhaps surprising that in spite of the two surfaces being in nominal contact over an elliptical area of about 2 mm^2 (within which there are several hundred prominent asperities on both surfaces) there are still significant “no-contact” periods, which strikingly demonstrates the underlying stiffness of the physical

micro-EHL system and its crucial role in protecting the surfaces even under the most severe conditions.

The strong dependence of contact and fatigue on the λ ratio predicted in the above and similar studies has encouraged the use of the ratio as the basis for a micropitting criterion. The use of a “specific lubricant film thickness” (similar in definition to the λ ratio) as the basis of a practical aid to avoid micropitting is embodied in a current ISO standard [40]. The document recognises that other specific factors, including lubricant chemistry, have an influence, but it is appreciated that the science has not developed sufficiently to allow such factors to be included directly in a calculation method. Thus the specific lubricant film thickness is recommended “as an evaluation criterion when applied as part of a suitable comparative procedure based on known gear performance”. It is therefore clear that gear practitioners recognise the need for a better understanding of the phenomenon of micropitting before it will be possible to provide a truly comprehensive design method to prevent it.

The experimental observation that running-in appears to occur almost instantaneously when new surfaces are put to work strongly suggests the important role of initial plastic deformation in determining the subsequent performance of gear teeth. Work has therefore been carried out on the elastic/plastic contact modelling of both single asperities and representative lengths of profiles from gear tooth surfaces to quantify the residual deformation and stress field. It was found that repeated elastic/plastic loading produces rapid shakedown which accords with the observed behaviour during running-in. The residual geometry and stress field obtained can, in principle, be incorporated into the micro-EHL simulations and elastic fatigue calculation, and work on this idea is ongoing. In pursuing this work a basic question to be answered is: does the residual stress field produced by initial plastic deformation significantly lengthen or shorten predicted fatigue life? Detailed examination of residual stress contours has revealed zones of high residual tensile stress very near to the surface and this may provide an explanation for the appearance of microcracks which then develop into micropitting.

A further mechanism which has been suggested as a factor affecting the propagation of surface micro-cracks is that of hydrostatic pressurisation of existing cracks by the EHL system. In classic early work on pitting under conditions of pure rolling involving more than eighty tests Dr Stewart Way [41, 42] of Westinghouse Laboratories, came to the remarkable conclusion that “pitting will not occur without lubricant”. By tracing the development of cracks Way found that pits initiated from minute cracks at the surface, and he proposed that the observed growth of the cracks under lubricated, but not dry, conditions was explained by the “theory of oil penetration”. Following Way several workers have produced models of crack pressurisation, a notable contribution was made by Bower [43] and more recently an EHL/crack pressurisation model has been proposed by Balcombe et al [44]. Opinions diverge on the issue of crack pressurisation, however, and it should be recalled that Way’s experiments were conducted under conditions of (almost) pure rolling, which is not the case in gears where micropitting is observed on the parts of the teeth where significant sliding occurs. It is clear that further work, involving both theoretical modelling and careful experimentation, will have to be carried out before the hypothesis can be proven or rejected. The challenge for numerical modellers is the full coupling of a transient micro-EHL solution with a consistent treatment of the mechanics of crack stressing and crack growth.

The work carried out by the Cardiff group on micropitting has been concerned with the physical mechanisms of EHL, elastic/plastic deformation and elastic fatigue damage modelling. The effects of surface chemistry and tribofilms has not been considered. In

eventually arriving at a full understanding of the problem of micropitting it is therefore believed that it will be necessary to combine the solid and fluid mechanics of rolling/sliding contacts with the behaviour of interacting surfaces at the molecular level.

8 Acknowledgements

Much of the research reported here was supported by the UK Engineering and Physical Sciences Research Council (EPSRC) with grants EP/G06024X/1 and EP/L021757/1, and the British Gear Association (BGA). We are also grateful to Design Unit of Newcastle University for supplying images of test gears.

9 References

- [1] Hohn BR, Oster, P, Emmert S. Micropitting in Case-Carburized Gears - FZG Micropitting Test, International Conference on Gears, VDI Berichte Nr. 1230, 331-334, Dresden, Germany, 1996.
- [2] Bell M, Sroka G, Benson R. The effect of the roughness profile on micropitting. *Gear Solutions*, March 2013: 47-53.
- [3] Brimble K, Atkins I, Blencoe, K, Aylott C, Shaw BA. A comparison of micropitting performance of identical oils using standard FZG test gears and helical test gears. *BGA Annual Congress*, 44-50, London, UK, 2001.
- [4] *Wind Turbine Micropitting Workshop: A Recap*, NREL Technical Report NREL/TP-500-46572 February 2010, (Shuangwen Sheng, Ed).
- [5] Errichello R, Sheng S, Keller J, Greco A. *Wind Turbine Tribology Seminar: A Recap*. National Renewable Energy Laboratory, Department of Energy Report DOE/GO-102012-3496 , February 2012
- [6] Dowson D, Higginson GR. *Elastohydrodynamic Lubrication*, Pergamon Press, Oxford, 1966
- [7] Holmes MJA, Qiao H, Evans HP, Snidle RW. Transient effects in EHL point and line contacts having rough transverse surface finish. Proc. 30th Leeds-Lyon Symp. on Tribology, Elsevier, Amsterdam, 201-212, 2004.
- [8] Chang L, Webster MN. A study of elastohydrodynamic lubrication of rough surfaces. *Trans ASME J Tribol* 1991; 113: 110-115.
- [9] Jiang X, Hua DY, Cheng HS, Ai X, Lee SC. Mixed elastohydrodynamic lubrication model with asperity contact. *Trans ASME J Tribol*. 1999; 121: 481-491.
- [10] Zhao J, Sadeghi F, Hoepfich MH. Analysis of EHL circular contact start up: Part I – mixed contact model with pressure and film thickness results. *Trans ASME J Tribol*. 2001; 123: 67-74.
- [11] Hu YZ, Zhu D. Full numerical solution to the mixed lubrication in point contacts. *Trans ASME J Tribol*. 2000; 122: 1-9.
- [12] Liu H, Mao K, Zhu C, Xu X. Mixed lubricated line contact analysis for spur gears using a deterministic model. *Trans ASME J Tribol*. 2012; 134: 021501-1 – 021501-7.
- [13] He T, Ren N, Zhu D, Wang J. Plasto-elastohydrodynamic lubrication in point contacts for surfaces with three-dimensional sinusoidal waviness and real machined roughness. *Trans ASME J Tribol*. 2014; 136: 031504-1 – 031504-11.

- [14] Hughes TG, Elcoate CD, Evans HP. Coupled solution of the elastohydrodynamic line contact problem using a differential deflection method. Proc IMechE, Part C: J Mech Eng Sci. 2000; 214: 585-598.
- [15] Elcoate CD, Evans HP, Hughes TG, Snidle RW. Transient elastohydrodynamic analysis of rough surfaces using a novel coupled differential deflection method. Proc IMechE Part J: J Eng Tribol. 2001; 215: 319-337.
- [16] Holmes MJA, Evans HP, Snidle RW. Analysis of mixed lubrication effects in simulated gear tooth contacts. Trans ASME J Tribol. 2005; 127: 61-69.
- [17] Holmes MJA, Evans HP, Hughes TG, Snidle RW. Transient elastohydrodynamic point contact analysis using a new coupled differential deflection method, Part 1: theory and validation. Proc IMechE, Part J: J Eng Tribol. 2003; 217: 289-303. Part 2: results. 305-321.
- [18] Evans HP, Sharif KJ, Snidle RW, Shaw BA, Zhang J. Analysis of micro-elastohydrodynamic lubrication and prediction of surface fatigue damage in micropitting tests on helical gears. Trans ASME J. Tribol. 2012; 135: 011501-011501-9.
- [19] Crook AW. Simulated gear tooth contacts: some experiments on their lubrication and subsurface deformations. Proc I Mech E. 1957; 171: 187-196.
- [20] Furey MJ. Metallic contact and friction between sliding surfaces. ASLE Trans. 1961; 4: 1-11.
- [21] Tallian TE, Chiu YP, Huttenlocher DF, Kamenshine JA, Sibley LB, Sindlinger NE. Lubricant films in rolling contact of rough surfaces. ASLE Trans. 1964; 7: 109-126
- [22] Leather JA, MacPherson PB. The practical use of electrical measurements in lubricated contacts. in: Dowson D, Taylor CM, Godet M, Berthe D, eds. Proc 4th Leeds-Lyon Symposium on Surface Roughness Effects in Lubrication, London MEP Ltd 1978 155.
- [23] Palacios JM. Elastohydrodynamic films in mixed lubrication: an experimental investigation. *Wear*. 1982; 89: 303
- [24] Guangteng G, Olver AV, Spikes H.A. Contact resistance measurements in mixed lubrication. In: *The Advancing Frontier of Engineering Tribology*, Proc. 1999 STLE/ASME. H.S.Cheng Tribology Surveillance 1999, Wang Q, Netzel J, Sadeghi F. eds, 64-71.
- [25] Lugt PM, Severt RWM, Fogelstro J, Tripp JH. Influence of surface topography on friction, film breakdown and running-in in the mixed lubrication regime. Proc I Mech E Part J, J Eng Tribol. 2001; 215: 519-533
- [26] Lord J, Larsson R. Film-forming capability in rough surface EHL investigated using contact resistance. Tribol Int. 2008; 41: 831-838.

- [27] Spikes HA, Guangteng G. An experimental study of film thickness in the mixed lubrication regime. in D Dowson, ed *Elastohydrodynamics '96: fundamentals and applications in lubrication and traction*. Amsterdam: Elsevier, 1997: 159-166.
- [28] Chittenden RJ, Dowson D, Dunn JF, Taylor CM. A theoretical analysis of the isothermal elastohydrodynamic lubrication of concentrated contacts. *Proc R Soc Lond*. 1985; A397: 245-269, 271-294.
- [29] Amzallag C, Gerey JP, Robert JL, Bahuaud J. Standardization of the rainflow counting method for fatigue analysis. *Int J Fatigue*.1994; 16: 287-293.
- [30] Qiao H, Evans HP, Snidle RW. Comparison of fatigue model results for rough surface elastohydrodynamic lubrication. *Proc IMechE Part J: J Eng Tribol*. 2008; 222: 381-393.
- [31] Fatemi A, Socie DF. A critical plane approach to multiaxial fatigue damage including out-of-phase loading. *Fatigue Fract Eng M*. 1988; 11: 149-165.
- [32] Zahavi E, Torbilo V. *Fatigue Design, Life Expectancy of Machine Parts*. CRC Press, Boca Raton,1996.
- [33] Qiao H. Prediction of contact fatigue for the rough surface elastohydrodynamic line contact problem under rolling and sliding conditions. PhD Thesis, Cardiff University, 2005.
- [34] Bishop IF, Snidle RW. Running-in of ground surfaces under elastohydrodynamic conditions. Paper No. 830310, Special Publication 539, *Studies of Engine Bearings and Lubrication*, Warrendale, 1983, Society of Automotive Engineers (SAE): 53-64.
- [35] Weeks IJJ. An Experimental Investigation into the Mixed Lubrication of Steel Surfaces, PhD thesis, Cardiff University, 2015.
- [36] Oila A, Shaw BA, Aylott CJ, Bull SJ. Martensite decay in micropitted gears. *Proc IMechE Part J: J Eng Tribol*. 2005; 219: 77-83.
- [37] Mulvihill DM, Kartal ME, Nowell D, Hills DA. An elastic-plastic asperity interaction model for sliding friction. *Tribol Int*. 2011; 44: 1679-1694.
- [38] Bryant MJ, Evans HP, Snidle RW. Plastic deformation in rough surface line contacts-a finite element study. *Tribol Int*. 2012; 46: 269-278.
- [39] Evans HP, Snidle RW, Sharif KJ, Bryant MJ. Predictive modelling of fatigue failure in concentrated lubricated contacts. *Faraday Discuss*. 2012; 156: 105-121.
- [40] International Standards Organisation. ISO/TR 15144-1:2014. *Calculation of micropitting load capacity of cylindrical spur and helical gears*. ISO, 2014.
- [41] Way S. Pitting due to rolling contact. *J Appl Mech*. 1935; 2: A49-A58
- [42] Way S. Gear tooth pitting. *The Electric Journal*. 1936; 33:175-177.
- [43] Bower AF. The influence of crack face friction and trapped fluid on surface initiated rolling contact fatigue cracks. *Trans ASME J Tribol*. 1988; 110: 704-711.
- [44] Balcombe R, Fowell MT, Olver AV, Ioannides S, Dini D. A coupled approach for rolling contact fatigue cracks in the hydrodynamic lubrication regime: The importance of fluid/solid interactions. *Wear*. 2011; 271:720-733.